Ultrasonics Sonochemistry 114 (2025) 107223

Contents lists available at ScienceDirect

Ultrasonics Sonochemistry

journal homepage: www.elsevier.com/locate/ultson

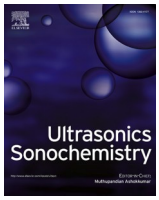

A flexible cystoscopy device prototype for mechanical tissue ablation based on micro-scale hydrodynamic cavitation: *Ex vivo* and *in vivo* studies

Ezgi Kestek [a,c,d,1], Ünal Akar [a,c,d,1], Seyedali Seyedmirzaei Sarraf [a,c,d,1], Ozcan Kanbur [b], Ufuk Gorkem Kirabali [b], Hande Eda Sutova [a], Morteza Ghorbani [a,c,d], Ozlem Kutlu [b,c], Huseyin Uvet [b], Asiye Isin Dogan Ekici [e], Sinan Ekici [c], Gül Kozalak [a,d,*], Ali Koşar [a,c,d,*]

[a] *Faculty of Engineering and Natural Sciences, Sabancı University, 34956 Tuzla, Istanbul, Turkey*
[b] *Department of Mechatronics Engineering, Yildiz Technical University, 34349 Besiktas, Istanbul, Turkey*
[c] *Sabancı University Nanotechnology Research and Application Center, 34956 Tuzla, Istanbul, Turkey*
[d] *Center of Excellence for Functional Surfaces and Interfaces for Nano-Diagnostics (EFSUN), Sabancı University, Orhanli, 34956 Tuzla, Istanbul, Turkey*
[e] *Acıbadem Mehmet Ali Aydınlar University, School of Medicine Department of Pathology, Ataşehir, 34755, Istanbul, Turkey*

ARTICLE INFO

Keywords:
Flexible Cystoscopy
Mechanical Tissue Ablation
Micro-Scale Hydrodynamic Cavitation
Ex vivo and *in vivo* Studies
Lower Urinary Tract Symptoms
Benign Prostatic Hyperplasia

ABSTRACT

Minimally invasive methods were sought for faster recovery from benign prostatic hyperplasia (BPH) and lower urinary tract (LUTS) symptoms. For this, the search for effective, low-side-effect methods for tissue ablation, particularly for managing BPH and certain bladder pathologies, has been continued to advance. In this regard, the energy released during the formation of hydrodynamic cavitation bubbles offers an alternative treatment method. In this study, we present the feasibility of the use of hydrodynamic cavitation with a flexible cystoscopy device prototype designed for the treatment of LUTS-related diseases. The developed flexible cystoscopy device prototype allows easy access to the urinary bladder through urethra with minimal pain, demonstrating its suitability as a minimally invasive approach. Precisely targeted cavitation exposure prevents prostatic capsule and bladder perforation. Moreover, an automatic actuating mechanism supports steering for real-time visual feedback. The developed device prototype was first tested on an ex vivo human bladder and then on an *in vivo* porcine bladder. Histopathological analyses were performed after both species were tested. For both analyses, significant tissue ablation at the targets was observed upon exposure to cavitating flows. Finally, the temperature profile on the device was obtained using a thermal camera. Accordingly, it was observed that the temperature increase during the procedure was not significant. The developed device prototype can thus realize mechanical ablation-based therapy, avoids unintended heat deposition which might appear in laser ablation and leads to fewer side effects such as uncontrolled tissue damage and low target area effectiveness that might occur in minimally invasive tissue ablation methods.

1. Introduction

Benign Prostatic Hyperplasia (BPH) is an urological disease that is frequently seen in men as they get older [1]. It is also known as prostate enlargement among the public and negatively affects the individual's life quality. Due to the expansion of prostate tissue, lower urinary tract symptoms (LUTS) occur as the bladder and other urethral tissues narrow [2]. Complaints in patients generally include sudden urination, nocturia, the feeling of not being able to empty the bladder, recurrent urinary tract infections and bladder stones [3]. Although BPH cannot be eliminated, its symptoms can be alleviated. BPH is a disorder that might lead to kidney failure if left untreated and affects 25.2 % of individuals [1]. Although the frequency of the disease increases with age, the highest prevalence is known to be above the age of 70 [4]. Alpha-blockers and alpha-reductase inhibitors are preferred as the first therapeutic approach [3]. Drug treatment facilitates urine flow by relaxing the smooth muscle tissues in the prostate and urinary tract. However, surgical intervention becomes inevitable in patients who do not respond to

* Corresponding authors.
E-mail addresses: gul.kozalak@sabanciuniv.edu (G. Kozalak), kosara@sabanciuniv.edu (A. Koşar).
[1] Co-first authors.

https://doi.org/10.1016/j.ultsonch.2025.107223
Received 18 July 2024; Received in revised form 18 December 2024; Accepted 3 January 2025
Available online 4 January 2025

medicaments [5]. There are several approaches to manage benign prostatic hyperplasia (BPH), each tailored to the severity of symptoms and patient needs. Two key approaches are debulking and ablation. Debulking procedures such as radical prostatectomy involve surgically removing part of the prostate and are commonly used in patients with larger prostates (greater than 80 mL) [6]. These procedures can reduce the tumor burden and increase the effectiveness of systemic treatments such as androgen deprivation in metastatic prostate cancer [7]. Ablation techniques are also minimally invasive procedures that aim to destroy excess prostate tissue or to reduce the prostate gland size. [8]. These techniques are preferred in patients with smaller prostate volumes or those who are not suitable for invasive surgeries due to advanced age or comorbidities [9]. Therefore, ablation is usually chosen for less severe cases or patients seeking for minimally invasive options, while debulking is reserved for more comprehensive disease management. [6].

In patients with excessive prostate enlargement, a suprapubic catheter can be used as a temporary solution before prostatectomy surgery. Depending on the condition of the patient, the surgeon can perform surgery to reduce the size of the prostate through the urethra or to widen the bladder neck. In both cases, the goal is to reduce the urinary complaints of the patient and to prevent bladder stones and kidney damage that might occur over time. Therefore, open or closed procedures can be used in surgical operations, but it has been reported that closed procedures provide faster recovery [10]. Extracorporeal and minimally invasive urological interventions are increasingly popular for treating kidney/bladder stones and abnormal genitourinary tissues [11,12].

Transurethral resection of the prostate (TURP) has historically been described as the gold standard and is frequently used for BPH [13]. In this procedure, special instruments are placed in the urethra to remove the enlarged parts of the prostate [14]. The procedure is performed within a short time and patients can return to their normal life the next day. Unfortunately, many complications occur after the operation, such as bleeding, sexual dysfunction, transurethral resection syndrome, urinary tract infection and urinary retention [5]. Monopolar and bipolar TURP efforts have shown equivalent complications [15]. Interest in this method of treating BPH has decreased since the 90 s with the emergence of alternative procedures [16]. For example, techniques based on ablation of the prostate using electricity, light or heat energy are preferred over TURP because they cause less bleeding [17]. In the plasma evaporation technique, the prostate tissue between the two electrodes is destroyed [18]. Laser enucleation is another ablation procedure of the prostate that is achieved with light energy [19]. Techniques used for laser ablation generally include photoselective vaporization (PVP), Holmium laser (HoLEP) and Thulium laser (THuLEP). In the high-intensity focused ultrasound (HIFU) technique, prostate-related tissues are targeted by using ultrasound waves [20]. On the other hand, some of the problems that may arise from laser ablation usage in TURP which are as follows; urinary retention, hematuria, infections and urethral strictures [21,22]. Histotripsy is primarily a non-thermal ablation method that uses short, focused ultrasound pulses to mechanically fractionate tissue via cavitation. While rapid, repeated pulses can produce localized heating under specific conditions [23], histotripsy protocols utilizing short pulses ($<$10 ms) have been shown to avoid thermal damage, generating precise and predictable ablation zones [24]. On the other hand, the transurethral needle ablation (TUNA) technique transmits low-energy radiofrequency waves through two needles to thermally ablate the prostate tissue [25]. TUNA may cause urinary retention, irritating symptoms, incomplete symptomatic relief, and a higher likelihood of retreatment [26,27]. In contrast to thermal ablation methods, mechanical ablation is less harmful to nearby cells and tissues and maintains the biological temperature in the vicinity of the exposed region [28]. For example, aquablation (Aquabeam®) is a heat-free tissue resection technique utilizing high-velocity waterjet with upstream pressures up to 55 MPa [29,30]. Another example involves the utilization of a two-stage cavitation strategy based on the sono-porosity effect for operating nanodroplet-coated microbubbles [31,32]. Theoretically, combining the effect of cavitation bubbles collapse with high-velocity jet flow augments the ablation efficacy and reduces the energy requirement for high pressures as in the case of waterjets. Hydrodynamic cavitation occurs when the local pressure of the liquid suddenly drops below the saturation vapor pressure. Hydrodynamic cavitation is obtained inside microchannels using microflow restrictive elements such as micro orifices, where the channel cross-section area suddenly shrinks [33]. Microscale hydrodynamic cavitation, which could be incepted with the use of micro-flow restrictive elements such as orifices, has shown a high potential for use in various bio-related applications [34]. Previous studies on harnessing the destructive energy of microscale hydrodynamic cavitation are promising [35].

While mechanical ablation elements brought together as a cystoscopy device, ergonomic factors had to be taken considered for operational safety. Urologists have to operate in a variety of distinctive ergonomic settings, each with its particular challenges. Surgeons might experience emotional fatigue, depersonalization, a lack of sense of personal accomplishment, and early retirement as a result of injuries [36]. The ergonomic factors in operational strategy can be counted as setting and exposure type, followed by device design and musculoskeletal alignment [37]. The height of the operating table is one of the most important parameters for achieving a neutral body position and also establishes the basis of all interactions. To maximize neutral position and minimize the surgeon discomfort, many studies reported that the operating surface height should be at the level of the groin symphysis of the surgeon or just below the elbow height [38]. At this height, the upper extremities remain at a neutral position for at least 90 % of the time, while muscle activation in the biceps is minimized [39]. When employing flexible ureteroscopic and cystoscopic equipment, much tension is put on the wrist and thumb. Accordingly, the extensor carpi ulnaris, thenar, and flexor carpi were reported to have the highest cumulative and average muscle workload for both navigation tasks and procedural activities. In contrast, the biceps, deltoid, and triceps had the lowest workload [40]. To reduce musculoskeletal strain, a variety of secure devices are available, each with benefits and drawbacks [41,42]. The performance of the system during cystoscopy must be improved by optimizing the cystoscope and endoscopy unit to reduce the risk of operation-related injuries and enhance the well-being of operators [37].

This study presents a unique, flexible cystoscopy device prototype based on hydrodynamic cavitation and offers an alternative treatment approach for lower urinary tract symptoms which is less invasive, more precise and user-friendly than existing approaches. To verify the efficacy of the cavitation probe as a biomedical device, it was initially assessed on an *ex vivo* human bladder and then on a male porcine bladder for modelling *in vivo*. The probe is housed in an 80° bendable, 3D-printed cystoscopy probe which is mounted on an automatic joystick. Moreover, an endoscopic camera was included to provide real-time guidance to the operator during *in vivo* porcine bladder. The proposed technique is safe and effective according to both the *ex vivo* human bladder and *in vivo* porcine bladder test results. The results provide an evidence for the biomedical use of this device in addressing lower urinary tract (LUTS) symptoms associated with BPH.

2. Material and methods

2.1. Device prototype and technological description

The device prototype was specifically designed and fabricated for *in vivo* porcine bladder tests to assess the effectiveness of microscale hydrodynamic cavitation on the mechanical ablation of soft tissues inside the urinary tract (Fig. 1D). The developed device consists of four different subsystems including a fluidic system (Fig. 1A), a flexible cystoscopy probe system (Fig. 1B), an actuation system (Fig. 1C), and a visualization system as included with other components in Fig. 1D.

The fluidic system, which provides the pressurized fluid flow essential for generating hydrodynamic cavitating flow, is composed of a

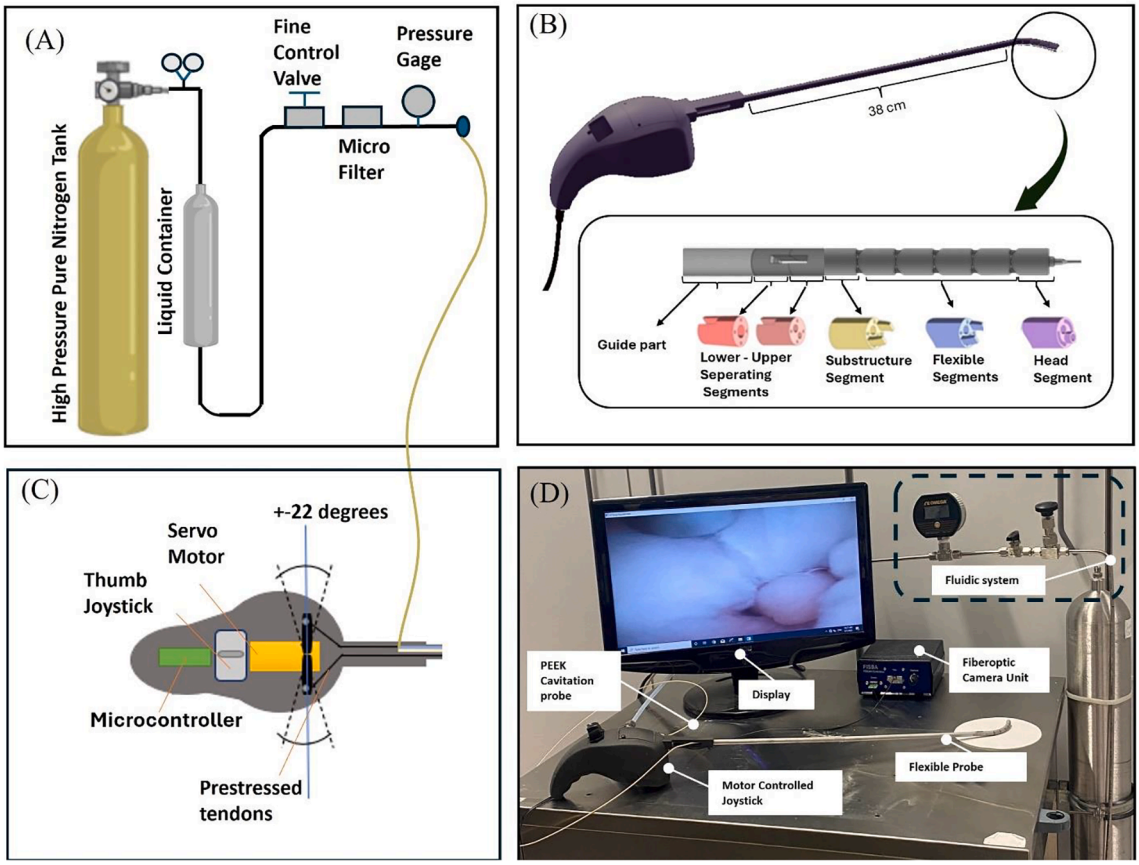

Fig. 1. Detailed schematic of the components of flexible cystoscopy device based on hydrodynamic cavitation **(A)** Schematic of the fluidic system to be used for cavitating flows **(B)** Cavitation probe inner, outer sections and flexible segments. **(C)** Motor controlled joystick components **(D)** Portable cystoscopy device equipped with hydrodynamic cavitation jet nozzle.

high-pressure nitrogen tank, a stainless-steel liquid container, stainless steel tubing, pressure gauges, a microparticle filter, control flow valves, and a biomedical grade flexible cavitation tube made of polyetheretherketone (PEEK) polymer. The flow restrictive element at the tip of the cavitation probe is a 1 cm long microtube with an inner diameter of 250 μm, which is attached to another PEEK tube with a length of 1.5 m and inner diameter of 1 mm. In order to determine the required upstream pressures corresponding to the formation and collapse of cavitation bubbles downstream of the nozzle, the submerged jet flow of the cavitation was experimentally visualized at various upstream pressures using a high-speed camera at 3000 frames per second (FPS). Further details can be found in Supplementary Information (S.I. 2). The real-time visualization system is composed of a 2 mm diameter camera module (FISCam™) with integrated illumination, which captures high-quality images with 400 × 400 resolution at 30 frames per second with a 120° field of view.

The cavitation probe and endoscopic camera were delivered and steered inside the urinary tract through a 3D-printed flexible cystoscopy probe. The fabricated cystoscope is a tendon-driven robotic platform comprised of three main sections including a guide part, a separating part, and a flexible part. The tendons used in the device are medical-grade stainless steel tendons. Pairs of tendons attaching to individual segments are common [43,44] as they facilitate autonomous movement of the segments. By adjusting the shear settings, it becomes possible to change the maximum angles at which joints can be bent, thereby enabling the constraint of bending capacities for each joint and the formulation of contact-aided compliant mechanisms (CCMs) [45]. Previous investigations by our group revealed that a bending angle of 5 degrees could be achieved at each junction in a total of 8 segments due to constraints related to the tooth-sleeve configuration [46]. In this study, one of our aims was to develop a new locking structure to achieve 8-degree bending angle in a single segment. Thus, a bending angle of 40 degrees could be reached with fewer segments in the tendon-driven mechanism. An increase in the number of segments in the flexible part leads to an increase in the bending angle as the total probe length decreases. Owing to the decreasing of the structure of the system, the guide part is composed of five separate pieces and constitutes a 38 cm long rigid insertion tube with a single hollow lumen at its center can be seen at bottom of the Fig. 1B. It is followed by a separating part where the cavitation probe and camera are segregated. The flexible part has a base piece, tiltable joint pieces, and a head segment. The bendable joints are tooth-sleeve structures, and each piece is limited to rotating 8° concerning the previous piece. The flexible part can bend up to ± 40° in a single axis with 5 connected segments at the distal tip. The head segment possesses two distinct engraved U-shaped trenches for tendon placements, thereby eliminating the need for tendon stopper ferrules. The total length of the probe is 46 cm, and its caliber is 21 FR (7 mm). In a previous study conducted by our research group, fabrication processes and preliminary attempts were included without a complete validation [47].

2.2. Forces acting on the end effector

Parameters such as flexibility, maneuverability and user-friendliness are very important during the design of the manipulator system. Flexible continuum robots exhibit a superior performance in terms of these parameters when compared to rigid body systems. Several major forces are acting on the flexible end effector which are shown in Fig. 2. $F_{tension}$ is the force resulting from the tension of the wires. F_j is the inertial force. F_{tube} is the counter force that occurs due to the deformation of the cavitation

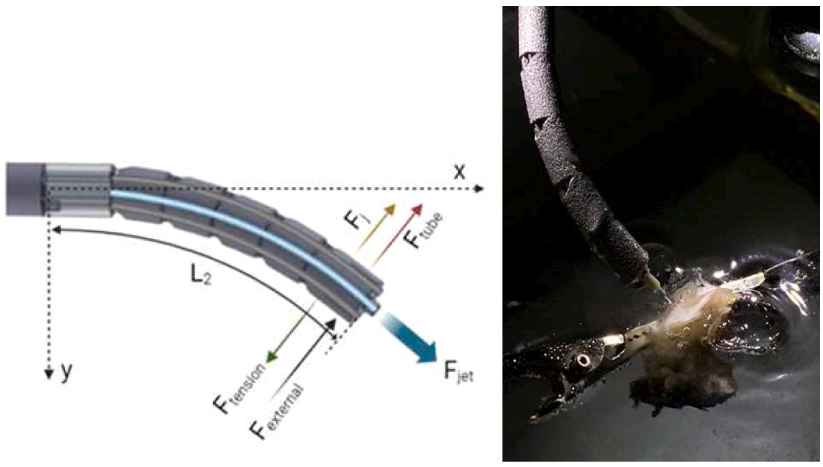

Fig. 2. Forces acting on the flexible part of the cystoscope and an image taken from the *ex vivo* human bladder.

tube material (Polyetheretherketone) during bending, which makes the elastic material return to its original shape. To generate hydrodynamic cavitation bubbles, the liquid inside the tube is propelled as the jet flows. A separate force arises from the contact of the liquid in the cavitation tube and the jet flow F_{jet}. This force introduces a Fluid-Structure Interaction (FSI) problem. Additionally, there are disruptive perturbations arising from this contact also shown as $F_{external}$.

The $F_{tension}$ applied for movement of the end effector is important to determine the robot's movement limits and field of view. According to the $F_{tension}$, the torque selection of the servo motor to be used in the prototype and other mechanical factors are determined. Therefore, the relationship between F_{tube} and F_{jet} force dynamics in the system needs to be known. Finally, there are friction forces that arise due to the mechanical contact between segments.

FSI emerges when a fluid flows through a deformable structure, resulting in an exchange of force and momentum between the two systems [48]. Initially, FSI studies focused on phenomena such as the water hammer effect and changes in fluid behavior under transient flows by taking the changes in tube wall thickness and tube deformation into account [49]. In general, when systems have fewer structural constraints, analyzing FSI becomes more crucial. The cavitation tube material is assumed to be linearly elastic in this regard. In the FSI analysis, various dimensionless parameters play important roles, including the Poisson's ratio, the ratio of pipe radius to tube wall thickness, ratio of liquid mass density to pipe wall mass density, ratio of liquid mass modulus to pipe wall thickness, Young's modulus, and ratio of liquid mass density to tube wall mass density. In addition, the behavior of an elastic tube subjected to continuous flow is affected by many parameters such as the fluid pressure, fluid velocity, forces acting on the tube, stresses and resonance frequencies of the materials. In order to understand this behavior, static and structural dynamic analysis of the flexible tube under various forces should be examined. There are two main approaches for transferring momentum to the structure: mechanical FSI and thermal FSI [50]. In our case, we investigate only mechanical FSI effects, neglecting the effect of heat on tube dynamics. In this study, a PEEK cavitation tube is considered. Periodic displacement is expected to occur at the free end of the tube due to jet flow. To analyze the force generated by the jet flow in the tube, we can examine the tube oscillation force caused by the jet flow in the end segment, considering that the bendable section is fixed at the base segment. Since the segments are freely movable, any FSI perturbation in the base segment is expected to affect all the subsequent segments. As the fluid leaves the tube, a reaction force occurs in the same direction as the flow direction of the fluid [51]. The variation method was used in the single-supported bendable tube-shaped model, and static effects were examined. The system converges or diverges at high flow rates with the FSI effect, depending on the dependent variables. w (x, T) represents the tube vibration [52]:

$$w(x,T) = \Sigma_w \sigma(x) e^{iwT} \tag{1}$$

According to sum of the w (x, T) values will grow exponentially, and the system will become imbalanced and divergent. By examining this limit, the maximum flow rate of the system can be calculated. The inlet velocity of the fluid, tube length and flexibility of the tube were selected as the major parameters. For the analysis, β value is obtained by calculating m_t and m_f which are the peek tube mass and DI water mass from the tube, respectively. The microtube at the tip is relatively short compared to the entire tubular cantilever and can be considered as a weight. The mass-dependent β value is between $0 < \beta < 1$. The β value for the cavitation tube can be expressed [53] as:

$$\beta = \frac{(m_f)}{(m_t + m_f)} \tag{2}$$

2.3. Motor driven actuating mechanism

A motor-driven mechanism was designed and developed to move the tendon-driven bending components of the flexible cystoscopy probe, which enables the operator to steer the cavitation probe onto the desired target. Savöx-1272SG servo motor with 30 kg-cm (294.2 N-cm) torque value at 7.4 V voltage supply was used in this system. By taking the operational requirements of surgeons during cystoscopy into account, a single-handed, user-friendly joystick was designed from scratch. The end effector can be controlled along one axis using a control knob and a servo motor. If necessary, the surgeon can easily rotate the joystick around 90° by turning the wrist or using the non-operating hand, allowing the end effector to reach intended areas in 3D space while receiving visual feedback from the endoscopic camera simultaneously. All required electronics were integrated into the joystick in a balanced manner, eliminating the need for an additional control box apart from energy input via a battery or DC adapter. Control algorithms were written in a C-based programming environment. The endoscopist's left hand is typically used to hold and operate cystoscopes. The operator may exert most of the force on a joint when it is in the neutral posture. Particular care could be taken when designing medical devices to ensure that the instrument is built to be utilized in a neutral posture. Implementing certain approaches is essential to ensure an ergonomically correct cystoscope which includes maintaining optimal handling, employing assisted torque vectoring, minimizing looping during the technique, and adopting a neutral grip. To enhance its sensitivity to tip deflection and torque, the cystoscope should be kept short and straight and have a flexible orientation. The prototype developed in this study allows the operator to use it with both right and left hands.

2.4. Patient and porcine samples

In the light of the experimental and numerical data obtained from previous studies conducted on a probe with an inner diameter close to that in this study (0.3 mm), it could be inferred that the pressure required for the cavitation inception should be higher than 0.55 MPa [54]. In addition, it was stated in the same study that the inlet pressure should be raised to the value of 1.035 MPa to reach the supercavitation condition [54]. Accordingly, the operation pressures were chosen as 0.35 MPa and 1.35 MPa to perform experiments under desired conditions. A bladder tissue sample from a male patient and a male porcine were used for the experimental study. The experimental protocols were approved by the institutional ethics committee for animal research of the Acibadem Mehmet Ali Aydinlar University (Ethic no: ACU-HADYEK 2020/06). The bladder tissue sample taken from the patient was excised in a triangular shape and stitched. Particular attention was paid to ensuring that the sample included the urethra and bladder neck. The human bladder sample was immediately placed in formalin, and the waiting time was 24 h for formalin fixation to occur. Before the flexible cystoscopy probe experiment, the tissue was soaked in Phosphate-Buffered Saline (PBS) for 1 h to rehydrate and purify it from formalin. The human bladder sample was divided into 5 sections and numbered, and no cavitation exposure was performed on the control sample. All procedures were applied to other samples from a distance probe top to the target of 3 mm and 20 min, the effect of the exposure was examined by changing the angle of the probe and the amount of pressure. For sample 3, the inlet pressure of angle of exposure of were applied 1.35 MPa and 0°, respectively, while they were 1.35 MPa and 40° for sample number 4, respectively. Samples 2 and 5 were tested by adjusted exposure angles to 0° and 40°, respectively at the inlet pressure of 0.35 MPa. The samples were examined under a Leica ES2 Stereo Microscope 10X before and after the cavitation process (Fig. 3, S.I. Fig. 1). To test the patient sample, the tissue should be tense, just like in a living body. A system, which can fulfil this function by pulling the tissue with 4 pegs and keeping it tense and stable, was designed (S.I. Fig. 2). The experiments were carried out in a tank filled with distilled water (DI) to represent the living body, and at this stage, it was recorded using the high-speed camera Dantec Speed Sense VEO 310 (S.I. 4).

For *in vivo* porcine bladder tests, a healthy male porcine with a body weight of 80 kg was used. The porcine was premedicated with 0.1 mg of diazepam per kilogram of body weight, 10 mg/kg ketamine, and 0.01 mg/kg atropine intramuscularly. Anaesthesia was induced with 2 mg/kg propofol administered intravenously. Following anaesthesia, porcine was draped and prepared for cystoscopy. During the operation (20 min.), the table height was set to 85 cm, and the distance from the monitor position to the front of the surgeon was fixed at 90 cm. To avoid any neck strain, the screen was fixed at 25° below the horizon to ensure an eye-resting position. The flexible cystoscopy probe was easily inserted through the urethra by using the flexibility feature. Cystoscopic examination and focus on urinary tissue were comfortably performed (Fig. 4A). The flexible hydrodynamic cavitation probe was easily localized on tissue for cavitation exposure (S.I. 5). Cystoscopy probe was applied to include the urethra and bladder neck of the porcine. After the cystoscopy procedure was completed, the porcine's abdomen was incised and its bladder was removed to demonstrate the efficiency of the probe through histopathological analysis (Fig. 4B). Then, a high dose of anesthetic was administered to the porcine.

2.5. Thermal Investigation of device prototype

The temperature profile around the device prototype and tissue samples was obtained using a thermal camera (FLIR T1020) to assess the temperature variations (Camera resolutions up to 1024x768, 3.1 MP). The thermal sensitivity of the camera was smaller 20 K at 30 °C, and the field of view was 12°x9°. The room temperature was fixed at 21 °C, thermal images with durations of 1and-5–10-15–20 min were taken on two different tissue samples for the inlet pressure of 0.35 MPa, where cavitation inception was not detected, as well as for the inlet pressure of 1.35 MPa, where the supercavitation condition existed. The aim of the temperature measurements was to identify the local temperature on the surface of the target tissue exposed to the emerging spray under the influence of cavitating flow inside the nozzle. The nozzle, specifically designed for this experiment, was positioned outside the water, while the target tissue was located in the vicinity of the liquid surface to facilitate accurate assessment of thermal effects. A thermal camera was placed one meter away from the experimental setup to track the heat generated by cavitation and transferred to the tissue. In order to capture temperature differences upon cavitation exposure, the camera focused on the spray and target's surface while recording temperature changes at the air–liquid interface. This experimental configuration addressed the drawbacks of direct temperature measurements within the liquid medium while detecting thermal dissipation caused by cavitation.

2.6. Histopathological analysis

The cavitation effect on the urethral samples was assessed by histopathological analysis of the specimens. The specimens were fixed in 10 % neutral buffered formalin for 24 h. All specimens were dissected into two pieces vertically from the middle of the cavitation region and at the same angle through a line bisecting the cavitation hole. All pieces were embedded in paraffin, sectioned in 3 μm thickness, and stained with Haematoxylin & Eosin. Evaluation of all specimens was histopathologically assessed by a digital image output from Virasoft software and interpreted by a pathologist. Histopathological images were analyzed in detail to extract such as penetration depth and ablation zone diameter in the ImageJ software.

2.7. Statistical analysis

For each histopathological image, penetration depth and ablation zone diameter were measured separately from 3 different slides. Student *t*-test was used to compare the results. The corresponding hypothesis can be expressed as: Do the effects of different angles differ on the penetration depth and ablation applied at the same pressure? All statistical

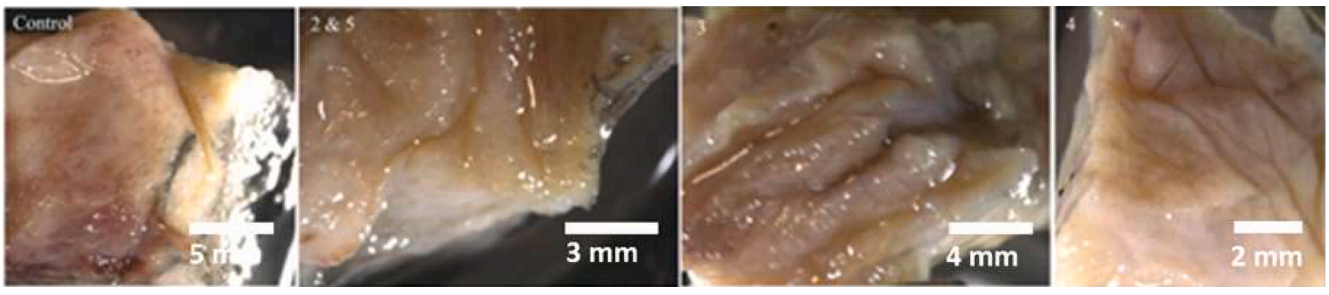

Fig. 3. Patient samples before the cavitation procedure.

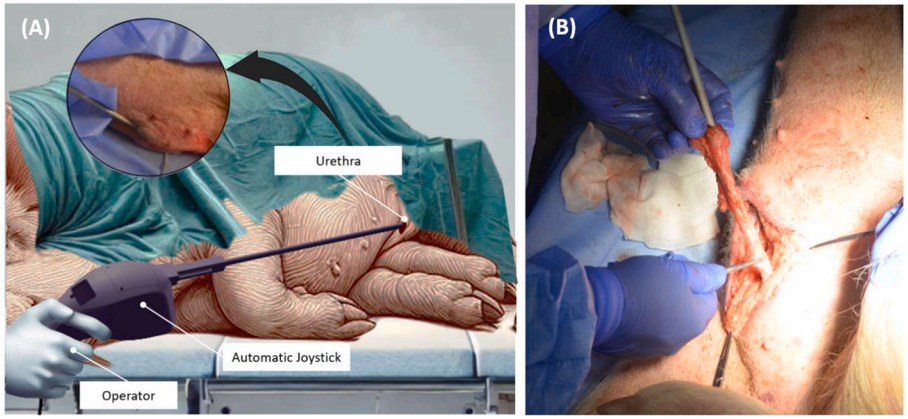

Fig. 4. **(A)** A schematic which represents the view of the operator during the ablation process with the flexible cystoscopy device with the cavitation effect placed in the urinary tract of the porcine. **(B)** The bladder removal process along with the urinary tract.

analyses were performed using the GraphPad Prism 5.01 (GraphPad Software Inc, Boston).

3. Results

3.1. Experimental investigation of the cavitation probe

The developed submerged jet corresponding to the smaller upstream pressure was associated with minimum disturbances. Fig. 5 represents ten consecutive frames for the upstream pressures of 0.7 MPa as the control case (no cavitation) and 1 MPa as the cavitating flow case where it was initially observed. At the same time, perturbations were observed at 1.66 msec, 2 msec, and 3 msec in the submerged jet at the larger upstream pressure indicating the collapse of cavitation bubbles inside the jet stream. Consequently, an increase in the upstream pressure intensifies the perturbations in the jet stream in response to the augmentation of vigorous cavitation bubble collapse. These results suggest that when considering the prototyped cavitation probe, an upstream pressure of 1 MPa or higher is required for creating cavitating flow downstream of the nozzle. In the light of all these results, the pressure value of 0.35 MPa was chosen as the reference pressure for presenting the non-cavitating flow condition. In addition, in order to amplify the ablation effect, the inlet pressure of 1.35 MPa was selected as the reference pressure for the supercavitation condition.

3.2. Validation of continuum robotic manipulator

According to the manufacturer's catalogue, the PEEK tube density ρ_{peek} is 1320 kg/m^3, the inner diameter of peek tube d_{in} is 1 mm, the outer diameter d_{out} is 1.6 mm. The tube length from base segment to tip L_1 is 90 mm, nozzle length L_n is 10 mm, nozzle inner diameter d_N is 0.8 mm. When β values are calculated according to L_1 length, β_2 can be found as 0.782. This value is between $0 < \beta < 1$. For this range, it can be stated that the flow is in the critical flow rate area. The imaginary part of the natural frequency becomes negative when fluid inflow velocity $u \geq 6$ m/s. In this case, the oscillation of the tube at $u > 6$ m/s is not convergent but rather divergent, which means that the tube oscillation becomes unstable above a certain flow rate [53]. Accordingly, the device was examined as submerged, and the system was operated at two different inlet pressure values, one low (0.35 MPa) and one high (1.35 MPa). It was observed that these conditions did not have any disruptive effect on the system's behavior. The minimum force needed to achieve the maximum joint angle (40°) was measured as 52.876 N for each pair of wires using a strain gauge during flow in the cavitation tube. Force and torque values measured at 10° intervals are given in Table 1.

In the torque calculation, a distance vector amplitude of 17 mm (the servo-horn torque distance) was considered so that the torque acting on each pair of wires could be computed as 89.889 N-cm. The proposed design effectively accommodates varying flow rates without the risk of divergent and unstable oscillations at the end effector. The tube's dynamics, including oscillations and other structural factors, can be controlled by adjusting flow rates and tube length, which enables a more efficient and effective device design. Ultimately, the measured and calculated values provide information for selecting an appropriate motor to achieve a bending angle of approximately 40°, thereby attaining the maximum joint angle. The motor-driven mechanism was embedded in an ergonomically designed and 3D printed joystick (190 mm × 70 mm) enabling the surgeon to maneuver single-handedly and to steer the distal part with only a push of a thumb. The device was tested by 3 different practitioners and it was observed that the highest tension was in the extensor pollicis brevis and abductor pollicis longus and lower in the extensor carpi ulnaris. The device is stabilized with a 15-20° grip between the operator and the handle while the operator is in a neutral position. The device can be rotated around 270° with the wrist. The designed device contributes to reducing the impact area of tension on the arm (255 g). More details are included in Supplementary Information 1 and 2. As a result of the force analysis and aforementioned efforts, a functional and ergonomic actuator system prototype was developed for surgical use, enabling the end effector to move via a servo motor. The presented motor-driven system facilitates the acquisition of images from various angles of the bladder with the flexible cystoscopy probe during the *in vivo* porcine bladder test (Fig. 6).

3.3. Temperature profile during operation

Thermal images of two different tissue samples are displayed in Fig. 7 for inlet pressures of 0.35 MPa and at 1.35 MPa. They were recorded using a thermal camera at exposure times of 1and-5–10–15–20 min. Detailed steps of experiment images taken at 1–5–10–15 and 20th minutes given in SI, Fig. 3. It can be clearly recognized that the temperatures within the tissue range from 22.50 °C to 23.90 °C. Moreover, the temperatures at the exit point of the nozzle vary from 21.90 °C to 25.10 °C. It can be inferred from the thermal data shown in Fig. 7 that the temperature changes in the vicinity of the tissue samples due to cavitating flow are relatively insignificant.

3.4. Histopathological analyses

The developed flexible cystoscopy probe was tested at inlet pressure of 0.35 MPa and 1.35 MPa exposure angles of 0° and 40° on patient samples. Then, it was utilized *in vivo* porcine bladder study on porcine under anaesthesia at inlet pressure of 1.35 MPa and exposure angle of

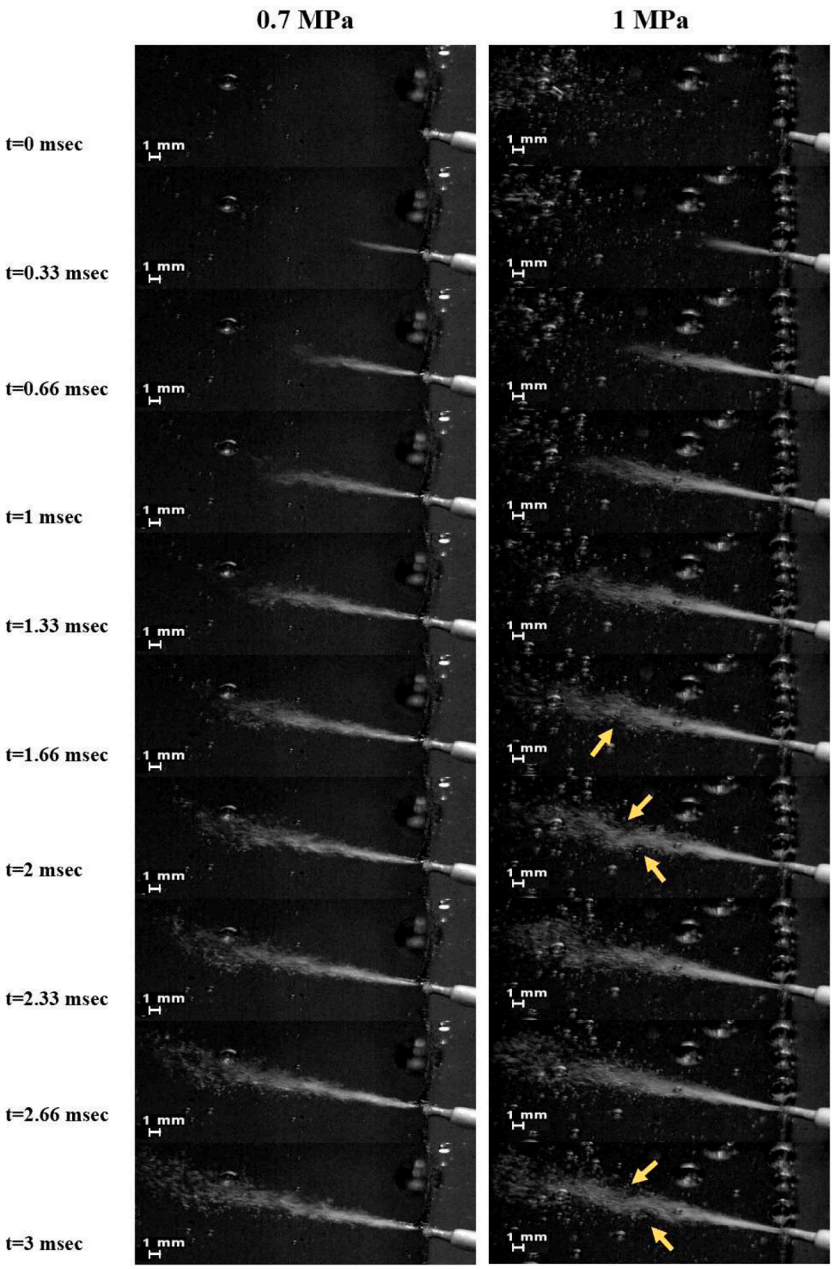

Fig. 5. High-speed visualization of submerged flows of the cavitation probe. Upstream pressures were obtained to study cavitating flow at 1 MPa (right) and non-cavitating flow at 0.7 MPa (left). At 1.66 ms, 2 ms, and 3 ms disturbances in the flow, indicated by yellow arrows, occurred due to the collapse of the cavitation bubbles and caused perturbations and locally curved streamlines.

Table 1
Force values measured at 10° intervals.

Bending angle	Mass (kg)	Force (N)	Torque (N-cm)
10°	1.28	12.557	21.347
20°	2.67	26.193	44.528
30°	3.25	31.882	54.199
40°	5.390	52.876	89.889

0°. Histopathological examination of porcine and human bladder tissues following ablation upon exposure to hydrodynamic cavitating flow reveals specific findings related to the ablation. In Fig. 8, the proposed device was used in an *ex vivo* human bladder which was performed under 0.35 MPa. No treatment was performed on the control sample. The non-cavitation condition was mimicked for both 0° and 40° bending angles. After 20 min of exposure time, no ablation was observed on the sample. As a result of histopathological analysis, 328.66 μm superficial ablations were observed in sample 0.35 MPa and 0° angle, while there wasn't depth detected. 355.68 μm depth was measured in sample 0.35 MPa and 0° angle. In the patient sample, only a superficial ablation of the bladder epithelium was observed at both 0° and 40° bending angles for 0.35 MPa pressure (Fig. 8).

Tissue ablation could be recognized for the inlet pressure of 1.35 MPa deep which can be observed from Fig. 9. Under the same pressure, 1.35 MPa, when the bending angle was 0°, the ablation surface diameter was 785.99 μm, and the depth of the ablation area was 635.21 μm. On the other hand, the ablation surface diameter was increased up to 1629. 71 μm and the ablation depth was decreased to 356.69 μm. As a result, cavitation-exposed areas could be seen eroded areas of the bladder mucosa, submucosa and deeper parts of lamina propria; characterized by loss of transitional cell layer, loss of connective tissue elements of

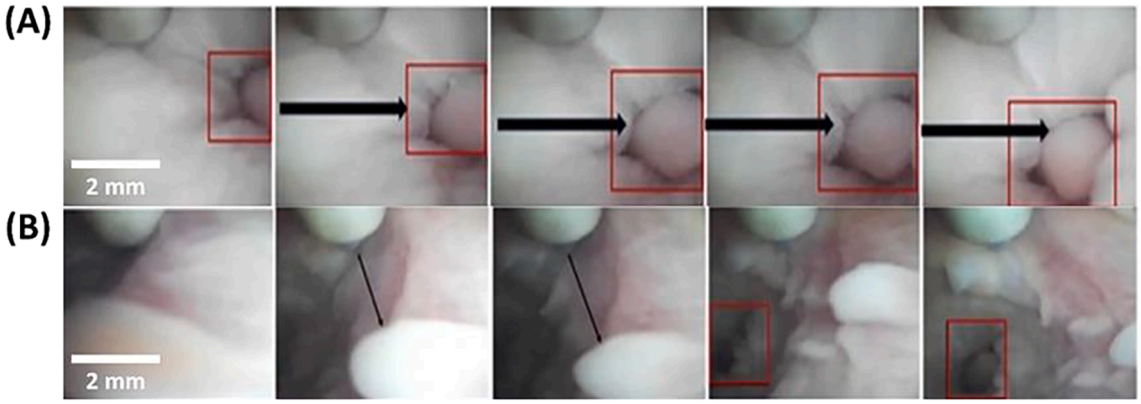

Fig. 6. **(A)** Right move and **(B)** Left move of the end effector.

submucosal area and deeper parts of lamina propria. Any findings of damage, erosion, necrosis or injury could not be seen in the neighbouring areas.

Based on this information, an *in vivo* porcine bladder was carried out on porcine at the inlet pressure of 1.35 MPa and bending angle of 0°. Histopathologic analyses show us the ablation surface diameter was 85.51 μm, and the depth of the ablation area was 337.73 μm. Hydrodynamic cavitation results in clear and prominent damage and loss of cells to the exposed urethral mucosa, and we can also detect the penetrating effect of cavitation into the deeper parts of the tissue such as submucosa and smooth muscle tissue (Fig. 10). It can be also observed that the application of cavitating flow leads to the formation of deeper and more focused and sharp areas of tissue damage in the target area.

Histopathological images were processed using the ImageJ program. The results are displayed in terms of penetration depth and ablation zone diameter in Table 2.

The results show only superficial ablation of the samples of the inlet pressure of 0.35 MPa and at both bending angles of 0° and 40° ($p < 0.0001$) (not shown graphic). According to *ex vivo* human bladder samples, the inlet pressure of 1.35 MPa and bending angle of 0° is more deep compared to the angle of 40° in 20 min. ($p < 0.0001$). According to the test results for the *in vivo* porcine bladder samples, the penetration deep generated by the cavitating flow at the inlet pressure of 1.35 MPa was measured as 337.73 μm within 20 min. Because penetration depth measurements are different between *ex vivo* human bladder and *in vivo* porcine bladder studies, there are statistically significant differences in the patient samples and porcine sample at the inlet pressure of 1.35 MPa and at the bending angle of 0° ($p < 0.0001$) (Fig. 11).

4. Discussion

BPH is a urological disorder seen in men over the age of 70 and often causes LUTS. The patient's complaints about urination increase and negatively affect the individual's life routine. While drug treatments provide fewer results in the long term, surgeries provide a significant increase in the quality of life in a short time. Bladder ablation is typically used in the standard management of BPH when LUTS are directly related to bladder pathology. In some cases where bladder function is compromised or additional bladder pathology is identified, bladder ablation may be considered to improve bladder emptying and to reduce symptoms [55]. Bladder outlet obstruction resulting from both prostatic enlargement and bladder neck dysfunction may require a combined approach to relieve symptoms [56]. Studies on bladder neck vaporization have shown that it improves overall urine flow and more rapidly reduces BPH symptoms [57,58]. These treatments are generally preferred when presenting with both BPH and LUTS and provide relief without extensive surgical procedures [59]. In addition, treating the bladder first minimizes complications from surgical procedures which are performed during prostate treatment [60]. In this sense, there is a need for biomedical devices that cause fewer side effects after the operation, provide recovery in a short time, and are also cheap and user-friendly. In this study, we explored the feasibility of harnessing the destructive energy of microscale hydrodynamic cavitation in urological soft tissue ablation.

We designed and developed a flexible cystoscopy device, which paves the way for a new treatment modality for patients with lower urinary tract symptoms. According to the conservation of mass and Bernoulli's principle, when a sudden cross-section reduction in the fluid flow's path happens, here along the small flow restrictive element which is the microtube at the tip of the nozzle, the fluid velocity increases, and the static pressure drops. The adjustment of the upstream pressure in the liquid container results in reaching the vapor pressure at the entrance of the microtube and the distal end of the nozzle. From these locations which act as nucleation sites, cavitation bubbles appear, grow, merge, and eject inside the submerged jet flow. When cavitation bubbles implode, the stored energy inside bubbles affects the nearby region and surface in terms of re-entrant jets and shock waves. Inertial cavitation and stable cavitation are two separate types that are commonly involved in ablation systems. When bubbles violently burst and rapidly expand due to drastic pressure fluctuations, inertial cavitation takes place, creating localized high temperatures and pressures that generate strong mechanical forces. Additionally, shockwaves released by their collapse intensify the mechanical disruption of adjacent tissues or materials [61,62]. On the other hand, the localized dissipation of energy by microstreaming and shear forces acting on surrounding structures occurs in stable cavitation, where bubbles oscillate around an equilibrium size without bursting. Stable cavitation is a supplementary mechanism in tissue manipulation because these oscillations contribute to mechanical or thermal effects over prolonged periods of time [63]. In hydrodynamic cavitation, both inertial and stable cavitation are essential because of their combined effects, which enable accurate and effective tissue ablation. The literature on ablation systems and cavitation-based technologies such as hydrodynamic sprays, ultrasound-induced cavitation, and other minimally invasive techniques for tissue disruption has extensively explained these mechanisms [64,65]. At the distal boundary of a collapsing bubble at its maximum volume, the re-entrant jet impinges towards the target tissue surface with a high velocity followed by the water hammer shock effect, which leads to the formation of primary shock waves. Subsequently, the cavitation bubble attains its minimum volume and collapses resulting in a secondary shockwave. The interaction of these shockwaves creates a high-pressure field, causing vigorous collapses of cavitation bubbles and high-velocity jets and imposing physical damage to the surface of the target tissue. To evaluate the *in vivo* efficacy of this approach, a flexible cystoscopy probe of 21 FR caliber and 80° bendability mounted on an automated joystick was designed and 3D printed. The cystoscopy device consisted of an

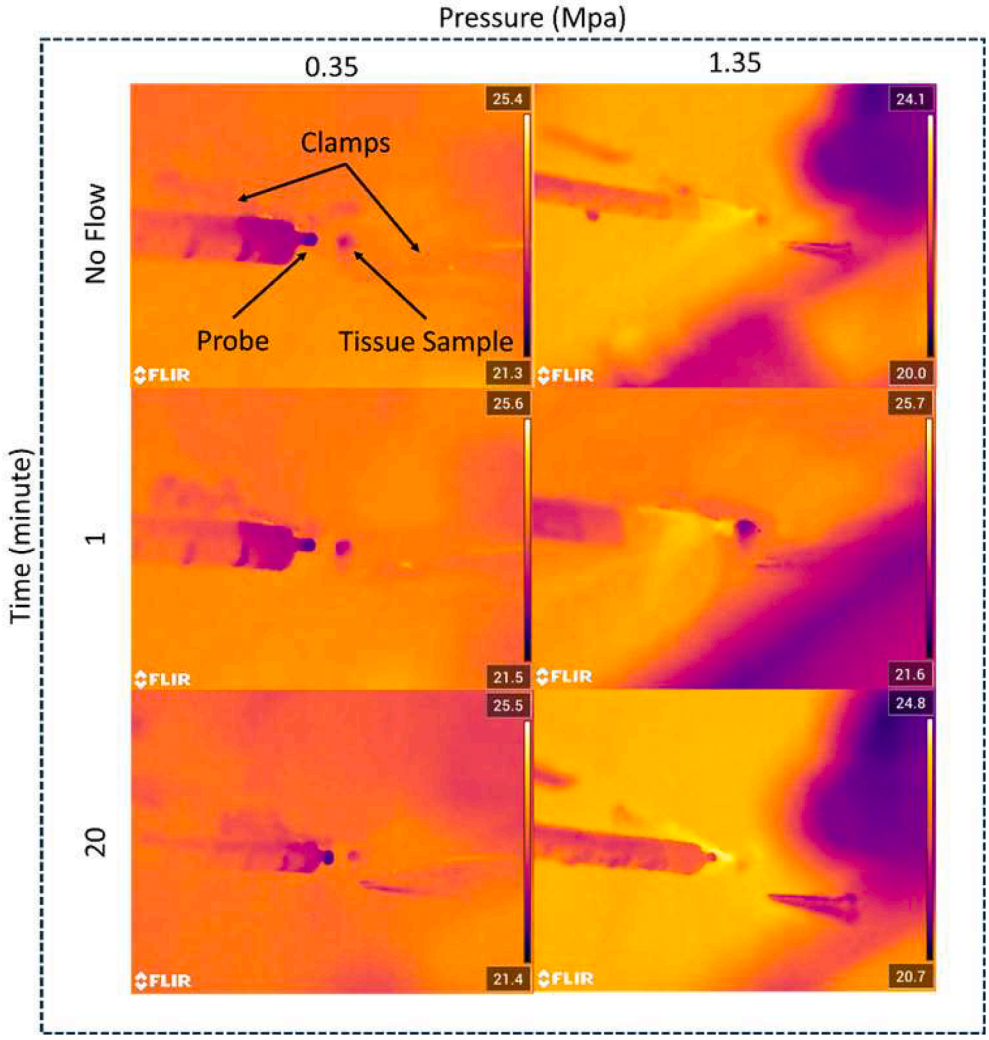

Fig. 7. Temperature distribution along the device neighborhood for different inlet pressures and durations.

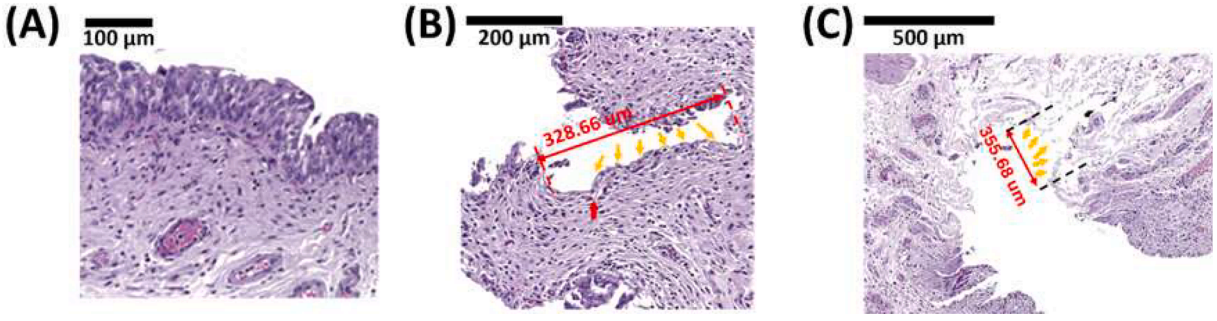

Fig. 8. Histological images of stained haematoxylin-eosin human bladder tissues. **(A)** Control **(B)** Cavitation zone at 0.35 MPa and bending angle of 0°. **(C)** Cavitation zone at 0.35 MPa and bending angle 40°.

endoscopic biomedical camera providing real-time visual feedback, as well as a prototyped flexible cavitation probe, which exposes cavitation flows inside the urinary system. The cavitation probe features a simple but effective micro orifice design consisting of a proximal fluid transmission line connected to a distal microtube tip, both made of PEEK material. The handheld motorized joystick provides a lightweight, portable, and ergonomic solution for guiding the cystoscopy probe within the urinary tract and targeting the site of exposure. Considering high-speed images of the submerged liquid flow at different operating upstream pressures of the cavitation probe, the flow disturbance due to cavitation bubble collapse in the flow was examined at 1 MPa, indicating the minimum required upstream pressure for delivering the cavitation bubbles out of the nozzle (Fig. 5). As a result, cavitating flow at the upstream pressure of 1.35 MPa was applied to the bladder tissues of both human and porcine.

Tested the developed biomedical device prototype first on *ex vivo* human bladder and then *in vivo* on porcine bladder. The porcine is often preferred because it can identify human diseases as a large animal model [66]. In *ex vivo* human bladder, only superficial ablation occurs of the inlet pressure of 0.35 MPa, while deep ablation occurs at the inlet

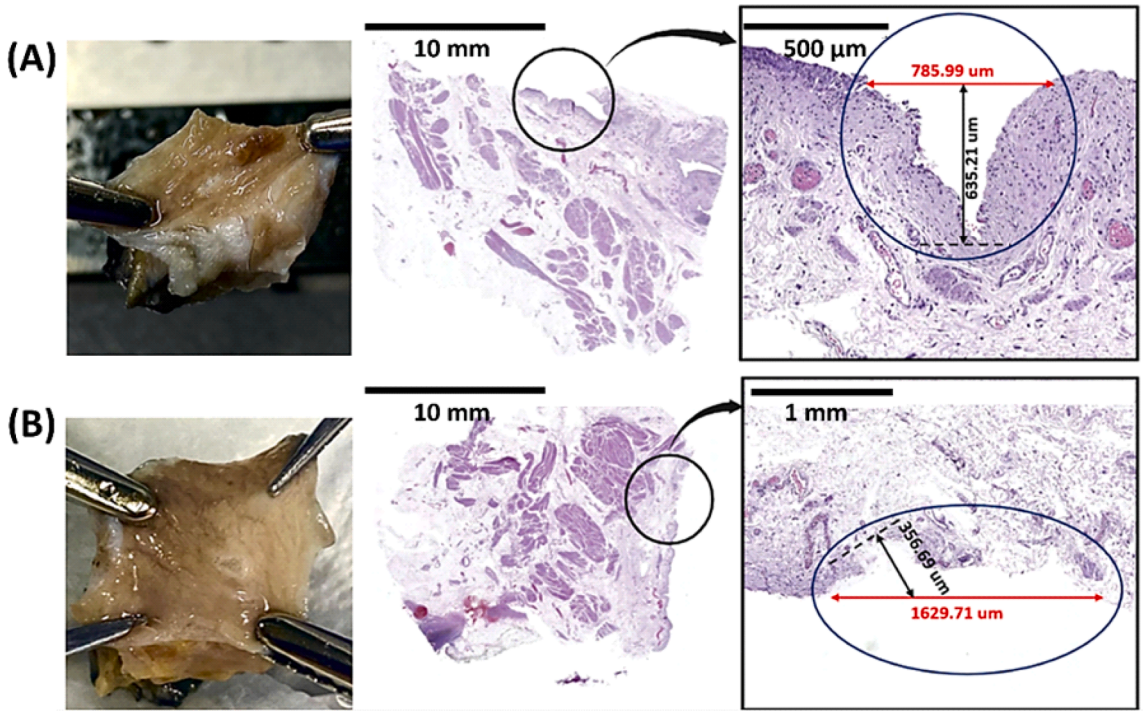

Fig. 9. Histological images of stained haematoxylin-eosin bladder tissues. Patient bladder specimen exposed to cavitation flow at 1.35 MPa **(A)** at 0° bending angle and **(B)** 40° bending angle.

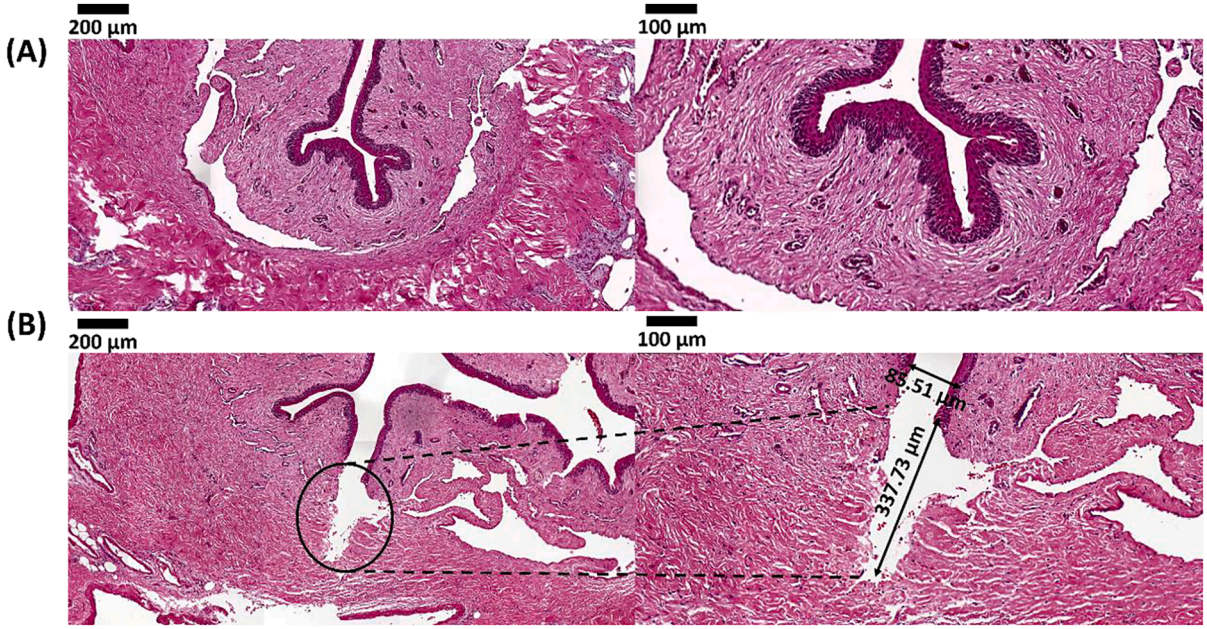

Fig. 10. Histological images of stained haematoxylin-eosin porcine bladder sample exposed to **(A)** non-cavitation flow and **(B)** cavitating flow at 1.35 MPa and bending angle 0°.

pressure of 1.35 MPa. In this case, the device is harmless at low pressures and shows the desired performance at higher pressures. After obtaining the optimum configuration at the inlet pressure of 1.35 MPa and bending angle of 0° *in vivo* porcine bladder tests were performed. Histopathological staining and analysis of the cavitation depths in porcine and human bladders differ significantly ($p < 0.0001$) (Fig. 11). The flexible cystoscopy probe created a 635.21 µm ablation depth when applied to the human bladder at the pressure of 1.35 MPa and bending angle of 0°, while the same pressure and angle applied to the porcine bladder resulted in a 337.73 µm ablation depth. This is due to the fact that porcine and human bladder tissues respond differently to low deformations due to the difference in elastin fiber network ratios [67]. In this sense, the behavior of porcine bladder tissues to mechanical effects is different from human bladder tissue [68,69]. Thus, the different results are due to differences between species [70]. Moreover, it is known that the bladder tissue in patients with diseases such as BPH and LUTS becomes thicker [71]. In addition, the water retention rate of living tissues and their different tensions in liquid may also be factors

Table 2
Ablation amounts of all specimens for *ex vivo* human bladder and *in vivo* porcine bladder.

Samples	Pressure	Bending Angle	Penetration Depth	Ablation Zone Diameter
Human bladder- 1	1.35 MPa	0°	635.21 μm	785.99 μm
Human bladder- 2	1.35 MPa	40°	356.69 μm	1629.71 μm
Human bladder- 3	0.35 MPa	0°	non	328.66 μm
Human bladder- 4	0.35 MPa	40°	non	355.68 μm
Porcine bladder	1.35 MPa	0°	337.73 μm	85.51 μm

contributing to this difference [72]. However, our *in vivo* porcine bladder test results provide positive outcomes and suggest that microscale hydrodynamic cavitation exposure achieves tissue ablation in both species, leading to tissue destruction in the targeted regions within 20 min. While radiofrequency and microwave ablation achieve larger lesion sizes (1.6–3.3 cm), they are associated with cooling water to avoid thermal damage for 5 min operation time which applied to a porcine liver [73]. Thulium fiber laser achieves a high ablation diameter (2.1–18 mm) with a better thermal control [74]. On the other side, our hydrodynamic cavitation approach provides a precise, localized ablation size (50 μm – 2.0 mm) with minimized surface thermal effects, making it a promising option for applications requiring high precision and minimal collateral damage. These observations indicate that hydrodynamic cavitation can induce controlled tissue damage in both porcine and human bladder tissues thanks to the designed and developed cystoscope prototype. We demonstrated the clinical usability of this device while our research efforts on developing the device are continuing.

Water jets have been utilized to cut soft tissues in a variety of scientific and clinical applications. According to studies, the pressure required for water jet cutting soft tissues with the Erbejet device ranges from 1 to 8 MPa [75,76]. During liver resection surgeries, average pressures range from 3 to 4 MPa [77]. In our case, we performed the whole experiment up to 1.35 MPa which helps to decrease the damage of neighboring tissue and cells. In similar studies conducted by our group, we found that the erosion rate of calcium oxalate kidney stone samples exposed to microscale hydrodynamic cavitation flows at the pressure of 9.79 MPa was 0.31 mg/min [78]. In addition, it was suggested that the distance, time and material properties between the micro orifice throat of the device and the sample could be correlated to estimate the erosion rate of kidney stones [79]. In another study, the effect of hydrodynamic cavitation flows at the pressure of 9.6 MPa on prostate cells and benign prostatic hyperplasia tissue was investigated and it was concluded that this approach was comparable to the ultrasonic cavitation method in the ablation of abnormal pathological tissues [80]. Besides, lithotripsy and cavitation-based methods used in the treatment of kidney stones were discussed and it was emphasized that hydrodynamic cavitation could be an alternative method to ultrasound-induced cavitation techniques in the treatment of kidney stones [17]. When immobilized cells are exposed to carpet bombardment with cavitation flows, the mechanical deformation and morphologies of various cancerous cell line differ [81]. The biophysical effect of HC on confluent cell monolayers was examined using the HC-on-a-chip device (HCOC) [82]. HC leads to different cellular response zones such as cell lysis, cell necrosis, cell permeabilization, and no-response region. In addition, it has been shown that oxidative stress occurs in the lysis and necrosis regions where bubble collapse occurs, and this has a destructive effect on structures such as membranes, DNA and protein. It has been shown that cell permeability increases and mechanical properties change in the zone between the HC-affected and unaffected regions [82]. While the effectiveness of reactive oxygen species (ROS) was not directly investigated, previous research has conducted similar examinations. In a study, ultrasonic pressure, radiation intensity and microbubble density were compared in mouse prostate xenograft tumors and it was shown that as the microbubble concentration increased, apoptosis increased [83]. The number of dead cells was compared by comparing the ceramide values that changed as a result of membrane disruption. Ceramide appears as a marker related to cell death. In this study, we examined the mechanical effect on the region of interest by using hematoxylin eosin staining. While the histopathological images provide insights into the condition of the cell cytoplasm and nuclei, it does not quantitively assess cell proliferation quantitatively. Future studies may include cell proliferation markers which will provide more detailed information about biophysical effects of cavitation bubbles as well as ROS effects. We recently developed a device prototype that is flexible and capable of hydrodynamic cavitation on a small scale [35]. The flexible cystoscopy prototype was tested in mouse models of prostate and bladder cancer and was reported to cause tissue damage in a short time [54]. The flow rate of the proposed system at a maximum pressure of 1.7 MPa was recorded at 3.67 ml/s according to a study published in a reputable journal [54]. In contrast, the Aquabeam device operates at a flow rate of 18.6 ml/s as indicated in another scholarly article [84]. The operation at such a high flow rate poses challenges in terms of flow control and potential harm to the surrounding tissues. Our system addresses these issues by offering a solution with a flow rate approximately 5 times slower, leading to minimal tissue damage compared to existing market solutions. The

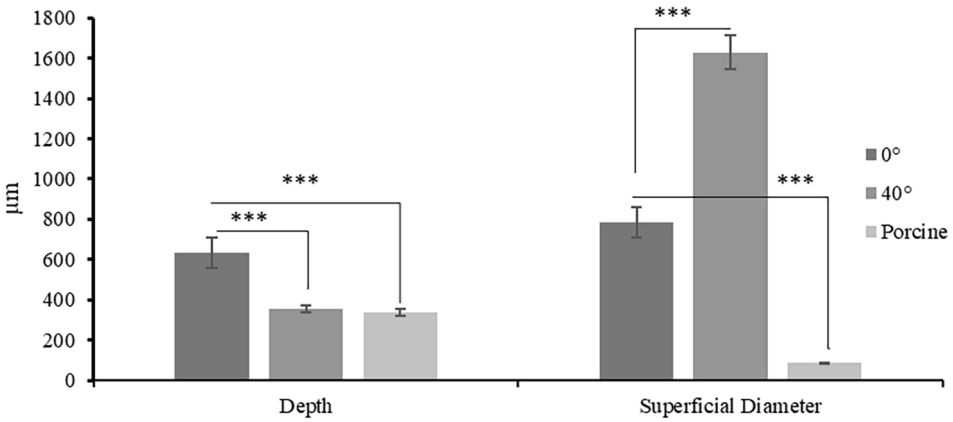

Fig. 11. Statistical comparison of human and porcine bladders under 1.35 MPa pressure ($p < 0.0001$).

Aquabeam device uses fluid jets for ablation, with an outer tube diameter of 22 Fr, an inner nozzle diameter of 330 μm, and operating pressures ranging from 3.45 MPa to 55.15 MPa [85]. This study proposed a device with a 21 Fr diameter and a microtube with an inner diameter of 250 μm, allowing for low-pressure hydrodynamic cavitation and preventing damage to surrounding tissues. The results of the performed *ex vivo* human bladder and *in vivo* porcine bladder tests demonstrate the feasibility of micro-scale hydrodynamic cavitation as a potential alternative method for treating LUTS symptoms in the bladder caused, for example, by BPH. The ablation rates are comparable with the related studies on high-pressure jets and ultrasound therapy [86,87]. Our device offers a unique approach for clinical use in sensitive and controlled tissue studies, minimizing the risk of undesired tissue damage. Furthermore, it will act as an alternative to existing methods that might cause thermal-induced unwanted tissue damage during ultrasound-induced cavitation. It can be used to treat various urological disorders and alleviate symptoms commonly seen in patients with BPH. Besides, the device provides a versatile and precisely controlled tissue removal targeting the bladder neck and bladder orifice to relieve bladder outlet obstruction (BOO).

The developed prototype stands out with its flexibility and user-friendly design, offering a minimally invasive approach for addressing LUTS symptoms in patients, including those caused by BPH. In addition, considering the concept of soft tissue ablation causing less damage to nearby tissue, it has a high potential for clinical use as a biomedical device. Further to its flexibility suitable for patients with small urethral canals, irrigation is not much needed since the device is fluid-powered. The mechanical ablation treatment performed by the device with hydrodynamic cavitation has fewer side effects because it is more targeted than other treatment procedures (radiofrequency, laser, ultrasound and cryoablation). Besides, it has been reported that medical treatment costs for patients are more expensive than surgery ($1,742 and $1,436, respectively) [88]. The cost of the developed flexible cystoscopy device is approximately $1000, excluding the endoscopic camera unit. In this sense, the developed device has a superior end-product cost when evaluated in terms of price performance. The developed flexible prototype has the potential of revolutionizing the management of LUTS, including symptoms associated with BPH, and will be further developed for commercialization and clinical use in the near future.

Author Contributions

E.K., U.A., S.S.S., G.K. wrote the original draft. E.K., U.A., O.K., U.G.K., H.E.S, M.G., O.U., H.U., A.I.D.E., S.E., G.K., A.K. did the conceptualization. E.K., U.K., S.S.S., O.K., U.G.K., H.E.S, M.G., O.K., H.U., A.I.D.E., S.E., A.K. contributed to the probe application principles. A.I.D.E. did histopathological analyses. S.E. did *in vivo* porcine experiments. E.K., U.A., G.K., O.K., U.G.K., H.E.S, M.G., O.U., H.U., A.I.D.E., S.E., A.K. did data curation and interpretation. M.G., O.K., H.U., A.I.D.E., S.E., G.K., A.K. edited the draft and revised the draft. S.E., A.K. obtained funding (TÜBİTAK Grant No. 118S040).

The manuscript was prepared with contributions from all the authors. All authors approved the final version of the manuscript.

CRediT authorship contribution statement

Ezgi Kestek: Writing – original draft, Visualization, Validation, Software, Methodology, Investigation, Formal analysis, Data curation. **Ünal Akar:** Visualization, Software, Methodology, Investigation, Formal analysis, Data curation. **Seyedali Seyedmirzaei Sarraf:** Writing – original draft, Software, Methodology, Investigation, Formal analysis, Data curation. **Ozcan Kanbur:** Software, Methodology, Formal analysis, Conceptualization. **Ufuk Gorkem Kirabali:** Visualization, Software, Methodology, Investigation, Data curation. **Hande Eda Sutova:** Validation, Methodology, Investigation, Formal analysis. **Morteza Ghorbani:** Writing – review & editing, Writing – original draft, Resources, Project administration, Methodology, Conceptualization. **Ozlem Kutlu:** Writing – original draft, Resources, Methodology, Investigation. **Huseyin Uvet:** Writing – original draft, Software, Resources, Methodology, Conceptualization. **Asiye Isin Dogan Ekici:** Writing – original draft, Resources, Methodology, Investigation, Formal analysis. **Sinan Ekici:** Writing – original draft, Project administration, Methodology, Funding acquisition, Formal analysis, Conceptualization. **Gül Kozalak:** Writing – review & editing, Writing – original draft, Validation, Supervision, Methodology, Investigation, Formal analysis, Data curation, Conceptualization. **Ali Koşar:** Writing – review & editing, Writing – original draft, Supervision, Resources, Project administration, Conceptualization.

Declaration of competing interest

The authors declare that this research was a collaborative effort supported by TÜBİTAK Grant No. 118S040, and funding was received starting from 2019. During the project, many students contributed thanks to the scholarship and completed their theses. The biomedical device concept was originally patented under the title ‘Apparatus for using hydrodynamic cavitation in medical treatment.’ (US8986322B2, EP2568893B1). Further advancements, including heat-based tests, robotics, imaging, micro-scale manipulation, and literature reviews, were carried out by the research team (authors). The authors affirm no commercial or financial conflicts of interest in publishing this work.

Acknowledgments

This study was supported by TÜBİTAK (The Scientific and Technological Research Council of Turkey) Support Program for Scientific and Technological Research Project Grant No. 118S040.

Appendix A. Supplementary data

Supplementary data to this article can be found online at https://doi.org/10.1016/j.ultsonch.2025.107223.

References

[1] S.W.H. Lee, E.M.C. Chan, Y.K. Lai, The global burden of lower urinary tract symptoms suggestive of benign prostatic hyperplasia: A systematic review and meta-analysis, Sci. Rep. 7 (1) (2017) 7984, https://doi.org/10.1038/s41598-017-06628-8.
[2] R.C. Langan, Benign Prostatic Hyperplasia, Prim. Care 46 (2) (2019) 223–232, https://doi.org/10.1016/j.pop.2019.02.003.
[3] S.D. Lokeshwar, B.T. Harper, E. Webb, A. Jordan, T.A. Dykes, D.E. Neal Jr, M. K. Terris, Z. Klaassen, Epidemiology and treatment modalities for the management of benign prostatic hyperplasia, Translational Andrology and Urology 8 (5) (2019) 529–539.
[4] J.V.A. Franco, P. Tesolin, J.H. Jung, Update on the management of benign prostatic hyperplasia and the role of minimally invasive procedures, Prostate Int. 11 (1) (2023) 1–7, https://doi.org/10.1016/j.prnil.2023.01.002.
[5] E.H. Kim, J.A. Larson, G.L. Andriole, Management of Benign Prostatic Hyperplasia, Annu. Rev. Med. 67 (2016) 137–151, https://doi.org/10.1146/annurev-med-063014-123902.
[6] B. Geavlete, F. Stanescu, C. Iacoboaie, P. Geavlete, Bipolar plasma enucleation of the prostate vs open prostatectomy in large benign prostatic hyperplasia cases - a medium term, prospective, randomized comparison, BJU Int. 111 (5) (2013) 793–803, https://doi.org/10.1111/j.1464-410X.2012.11730.x.
[7] G. Swanson, I. Thompson, J. Basler, E.D. Crawford, Metastatic prostate cancer-does treatment of the primary tumor matter? J. Urol. 176 (4 Pt 1) (2006) 1292–1298, https://doi.org/10.1016/j.juro.2006.06.069.
[8] P. Thurmond, S. Bose, L.B. Lerner, Holmium laser for the surgical treatment of benign prostatic hyperplasia, Can. J. Urol. 23 (4) (2016) 8356–8362.
[9] P. Grise, M. Plante, J. Palmer, J. Martinez-Sagarra, C. Hernandez, M. Schettini, M. Gonzalez-Martin, J. Castiñeiras, P. Ballanger, P. Teillac, F. Rolo, V. Baena, J. Erdmann, V. Mirone, Evaluation of the transurethral ethanol ablation of the prostate (TEAP) for symptomatic benign prostatic hyperplasia (BPH): a European multi-center evaluation, Eur Urol 46(4) (2004) 496-501; discussion 501-2. 10.1016/j.eururo.2004.06.001.
[10] S. Rojanasarot, B. Cutone, K. Durand, K.C. Zorn, B. Chughtai, N. Bhojani, D. S. Elterman, Patients' Perspectives on Attributes While Choosing Minimally Invasive Surgery for Benign Prostatic Hyperplasia Procedures: Experience from

Men Undergoing Water Vapor Thermal Therapy, J. Endourol. 37 (5) (2023) 575–580, https://doi.org/10.1089/end.2022.0607.
[11] P.F. Müller, D. Schlager, S. Hein, C. Bach, A. Miernik, D.S. Schoeb, Robotic stone surgery - Current state and future prospects: A systematic review, Arab. J. Urol. 16 (3) (2018) 357–364, https://doi.org/10.1016/j.aju.2017.09.004.
[12] J. Panzone, T. Byler, G. Bratslavsky, H. Goldberg, Applications of Focused Ultrasound in the Treatment of Genitourinary Cancers, Cancers (basel) 14 (6) (2022), https://doi.org/10.3390/cancers14061536.
[13] M.J. Young, M. Elmussareh, T. Morrison, J.R. Wilson, The changing practice of transurethral resection of the prostate, Ann. R. Coll. Surg. Engl. 100 (4) (2018) 326–329, https://doi.org/10.1308/rcsann.2018.0054.
[14] B. Chughtai, S. Rojanasarot, K. Neeser, D. Gultyaev, S. Fu, S.K. Bhattacharyya, A. M. El-Arabi, B.J. Cutone, K.T. McVary, A comprehensive analysis of clinical, quality of life, and cost-effectiveness outcomes of key treatment options for benign prostatic hyperplasia, PLoS One 17 (4) (2022) e0266824.
[15] C.E. Méndez-Probst, L. Nott, S.E. Pautler, H. Razvi, A multicentre single-blind randomized controlled trial comparing bipolar and monopolar transurethral resection of the prostate, Can. Urol. Assoc. J. 5 (6) (2011) 385–389, https://doi.org/10.5489/cuaj.10199.
[16] B. Rocco, G. Albo, R.C. Ferreira, M. Spinelli, G. Cozzi, P. Dell'orto, V. Patel, F. Rocco, Recent advances in the surgical treatment of benign prostatic hyperplasia, Ther. Adv. Urol. 3 (6) (2011) 263–272, https://doi.org/10.1177/1756287211426301.
[17] M. Ghorbani, O. Oral, S. Ekici, D. Gozuacik, A. Kosar, Review on Lithotripsy and Cavitation in Urinary Stone Therapy, IEEE Rev. Biomed. Eng. 9 (2016) 264–283, https://doi.org/10.1109/rbme.2016.2573381.
[18] H. Aboutaleb, Efficacy of bipolar "button" plasma vaporization of the prostate for benign prostatic obstruction, compared to the standard technique, Urol Ann 7 (4) (2015) 442–447, https://doi.org/10.4103/0974-7796.152019.
[19] X. Qian, H. Liu, D. Xu, L. Xu, F. Huang, W. He, J. Qi, Y. Zhu, D. Xu, Functional outcomes and complications following B-TURP versus HoLEP for the treatment of benign prostatic hyperplasia: a review of the literature and Meta-analysis, Aging Male 20 (3) (2017) 184–191, https://doi.org/10.1080/13685538.2017.1295436.
[20] D. Cranston, T. Leslie, G. Ter Haar, A Review of High-Intensity Focused Ultrasound in Urology, Cancers (basel) 13 (22) (2021), https://doi.org/10.3390/cancers13225696.
[21] M.J. James, D.R. Harriss, A. Ceccherini, A.R. Manhire, C.P. Bates, A urodynamic study of laser ablation of the prostate and a comparison of techniques, Br. J. Urol. 76 (2) (1995) 179–183, https://doi.org/10.1111/j.1464-410x.1995.tb07670.x.
[22] R.S. Cowles 3rd, J.N. Kabalin, S. Childs, H. Lepor, C. Dixon, B. Stein, A. Zabbo, A prospective randomized comparison of transurethral resection to visual laser ablation of the prostate for the treatment of benign prostatic hyperplasia, Urology 46 (2) (1995) 155–160, https://doi.org/10.1016/s0090-4295(99)80185-x.
[23] Y.N. Wang, T.D. Khokhlova, S. Buravkov, V. Chernikov, W. Kreider, A. Partanen, N. Farr, A. Maxwell, G.R. Schade, V.A. Khokhlova, Mechanical decellularization of tissue volumes using boiling histotripsy, Phys. Med. Biol. 63 (23) (2018) 235023, https://doi.org/10.1088/1361-6560/aaef16.
[24] Y.N. Wang, T. Khokhlova, M. Bailey, J.H. Hwang, V. Khokhlova, Histological and biochemical analysis of mechanical and thermal bioeffects in boiling histotripsy lesions induced by high intensity focused ultrasound, Ultrasound Med. Biol. 39 (3) (2013) 424–438, https://doi.org/10.1016/j.ultrasmedbio.2012.10.012.
[25] F. Aoun, Q. Marcelis, T. Roumeguère, Minimally invasive devices for treating lower urinary tract symptoms in benign prostate hyperplasia: technology update, Res Rep Urol 7 (2015) 125–136, https://doi.org/10.2147/rru.S55340.
[26] Y.X.T. Law, W.J.K. Chen, L. Shen, W.J. Chua, Is transurethral needle ablation of prostate out of fashion? Outcomes of Single Session Office-Based Transurethral Needle Ablation of Prostate in Patients with Symptomatic Benign Prostatic Hyperplasia, Investig Clin Urol 60 (5) (2019) 351–358, https://doi.org/10.4111/icu.2019.60.5.351.
[27] J.N. Cornu, F. Desgrandchamps, A. de la Taille, E. Vicaut, M. Aout, B. Lukacs, Prospective short-term evaluation of transurethral needle ablation procedure in an ambulatory setting, Urol. Int. 89 (4) (2012) 451–456, https://doi.org/10.1159/000342362.
[28] G. Mauri, L. Nicosia, Z. Xu, S. Di Pietro, L. Monfardini, G. Bonomo, G.M. Varano, F. Prada, P. Della Vigna, F. Orsi, Focused ultrasound: tumour ablation and its potential to enhance immunological therapy to cancer, Br. J. Radiol. 91 (1083) (2018) 20170641, https://doi.org/10.1259/bjr.20170641.
[29] K. Faber, A.L. de Abreu, P. Ramos, N. Aljuri, S. Mantri, I. Gill, O. Ukimura, M. Desai, Image-guided robot-assisted prostate ablation using water jet-hydrodissection: initial study of a novel technology for benign prostatic hyperplasia, J. Endourol. 29 (1) (2015) 63–69, https://doi.org/10.1089/end.2014.0304.
[30] P. Gilling, R. Reuther, A. Kahokehr, M. Fraundorfer, Aquablation - image-guided robot-assisted waterjet ablation of the prostate: initial clinical experience, BJU Int. 117 (6) (2016) 923–929, https://doi.org/10.1111/bju.13358.
[31] Y. Pan, Y. Li, Y. Li, X. Zheng, C. Zou, J. Li, H. Chen, Nanodroplet-Coated Microbubbles Used in Sonothrombolysis with Two-Step Cavitation Strategy, Adv. Healthc. Mater. 12 (6) (2023) e2202281.
[32] Y. Pan, Y. Li, Y. Chen, J. Li, H. Chen, Dual-Frequency Ultrasound Assisted Thrombolysis in Interventional Therapy of Deep Vein Thrombosis, Adv. Healthc. Mater. 13 (9) (2024) e2303358.
[33] A. Koşar, M. Şeşen, O. Oral, Z. Itah, D. Gozuacik, Bubbly cavitating flow generation and investigation of its erosional nature for biomedical applications, I.E.E.E. Trans. Biomed. Eng. 58 (5) (2011) 1337–1346, https://doi.org/10.1109/tbme.2011.2107322.
[34] S. Seyedmirzaei Sarraf, F. Rokhsar Talabazar, I. Namli, M. Maleki, A. Sheibani Aghdam, G. Gharib, D. Grishenkov, M. Ghorbani, A. Koşar, Fundamentals, biomedical applications and future potential of micro-scale cavitation-a review, Lab on a Chip 22(12) (2022) 2237-2258. 10.1039/D2LC00169A.
[35] M. Ghorbani, C. Sozer, G. Alcan, M. Unel, S. Ekici, H. Uvet, A. Koşar, Biomedical device prototype based on small scale hydrodynamic cavitation, AIP Adv. 8 (3) (2018) 035108, https://doi.org/10.1063/1.5005048.
[36] Y. Mizuno, H. Narimatsu, Y. Kodama, T. Matsumura, M. Kami, Mid-career changes in the occupation or specialty among general surgeons, from youth to middle age, have accelerated the shortage of general surgeons in Japan, Surg. Today 44 (4) (2014) 601–606, https://doi.org/10.1007/s00595-013-0613-6.
[37] A.T. Gabrielson, M.M. Clifton, C.P. Pavlovich, M.J. Biles, M. Huang, J. Agnew, P. M. Pierorazio, B.R. Matlaga, P. Bajic, Z.R. Schwen, Surgical ergonomics for urologists: a practical guide, Nat. Rev. Urol. 18 (3) (2021) 160–169, https://doi.org/10.1038/s41585-020-00414-4.
[38] R. Berquer, W.D. Smith, S. Davis, An ergonomic study of the optimum operating table height for laparoscopic surgery, Surg. Endosc. 16 (3) (2002) 416–421, https://doi.org/10.1007/s00464-001-8190-y.
[39] M.A. van Veelen, G. Kazemier, J. Koopman, R.H. Goossens, D.W. Meijer, Assessment of the ergonomically optimal operating surface height for laparoscopic surgery, J. Laparoendosc. Adv. Surg. Tech. A 12 (1) (2002) 47–52, https://doi.org/10.1089/109264202753486920.
[40] W.W. Ludwig, G. Lee, J.B. Ziemba, J.S. Ko, B.R. Matlaga, Evaluating the Ergonomics of Flexible Ureteroscopy, J. Endourol. 31 (10) (2017) 1062–1066, https://doi.org/10.1089/end.2017.0378.
[41] S.N. El-Tallawy, R. Nalamasu, G.I. Salem, J.A.K. LeQuang, J.V. Pergolizzi, P. J. Christo, Management of Musculoskeletal Pain: An Update with Emphasis on Chronic Musculoskeletal Pain, Pain Ther. 10 (1) (2021) 181–209, https://doi.org/10.1007/s40122-021-00235-2.
[42] V.C. Hoe, D.M. Urquhart, H.L. Kelsall, E.N. Zamri, M.R. Sim, Ergonomic interventions for preventing work-related musculoskeletal disorders of the upper limb and neck among office workers, Cochrane Database Syst. Rev. 10 (10) (2018) Cd008570, https://doi.org/10.1002/14651858.CD008570.pub3.
[43] D. Ji, T.H. Kang, S. Shim, S. Lee, J. Hong, Wire-driven flexible manipulator with constrained spherical joints for minimally invasive surgery, Int. J. Comput. Assist. Radiol. Surg. 14 (8) (2019) 1365–1377, https://doi.org/10.1007/s11548-019-01976-4.
[44] Y. Kim, S.S. Cheng, J.P. Desai, Active Stiffness Tuning of a Spring-based Continuum Robot for MRI-Guided Neurosurgery, IEEE Trans. Rob. 34 (1) (2018) 18–28, https://doi.org/10.1109/tro.2017.2750692.
[45] N.D. Mankame, G.K. Ananthasuresh, Contact Aided Compliant Mechanisms: Concept and Preliminaries (2002) 109–121.
[46] C. Sozer, M. Ghorbani, G. Alcan, H. Uvet, M. Unel, A. Kosar, Design, Prototyping and Control of a Flexible Cystoscope for Biomedical Applications, IOP Conf. Ser.: Mater. Sci. Eng. 224 (1) (2017) 012050, https://doi.org/10.1088/1757-899X/224/1/012050.
[47] S.S. Sarraf, New-generation 3D Printed Biomedical Device Based on Micro-scale Hydrodynamic Cavitation, Sabanci University, 2022.
[48] D.C. Wiggert, A.S. Tijsseling, Fluid transients and fluid-structure interaction in flexible liquid-filled piping, Appl. Mech. Rev. 54 (5) (2001) 455–481, https://doi.org/10.1115/1.1404122.
[49] R. Skalak, An Extension of the Theory of Water Hammer, Trans. Am. Soc. Mech. Eng. 78 (1) (2022) 105–115, https://doi.org/10.1115/1.4013579.
[50] C.G. Giannopapa, Fluid structure interaction in flexible vessels, Technische Universiteit Eindhoven, CASA-report; Vol. 0622, 2006.
[51] A.S. Tijsseling, FLUID-STRUCTURE INTERACTION IN LIQUID-FILLED PIPE SYSTEMS: A REVIEW, J. Fluids Struct. 10 (2) (1996) 109–146, https://doi.org/10.1006/jfls.1996.0009.
[52] M.P. Païdoussis, G.X. Li, Pipes Conveying Fluid: A Model Dynamical Problem, Journal of Fluids and Structures 7(2) (1993) 137–204, https://doi.org/10.1006/jfls.1993.1011.
[53] R.W. Gregory, M.P. Paidoussis, W.R. Hawthorne, Unstable oscillation of tubular cantilevers conveying fluid II. Experiments, Proceedings of the Royal Society of London. Series A. Mathematical and Physical Sciences 293(1435) (1997) 528-542. 10.1098/rspa.1966.0188.
[54] T. Abbasiasl, H. Sutova, S. Niazi, G. Celebi, Z. Karavelioglu, U. Kirabali, A. Yilmaz, H. Uvet, O. Kutlu, S. Ekici, M. Ghorbani, A. Kosar, A Flexible Cystoscope Based on Hydrodynamic Cavitation for Tumor Tissue Ablation, I.E.E.E. Trans. Biomed. Eng. 69 (1) (2022) 513–524, https://doi.org/10.1109/tbme.2021.3100542.
[55] G. de la Torre, G. Barusso, V. Chernobilsky, M. Borghi, L. Montes de Oca, E. Becher, Outpatient simultaneous treatment of benign prostatic hyperplasia and bladder lithiasis with GreenLight™ and holmium laser, J. Endourol. 26 (2) (2012) 164–167, https://doi.org/10.1089/end.2011.0249.
[56] T. McNicholas, R. Kirby, Benign prostatic hyperplasia and male lower urinary tract symptoms, Am Fam Physician 86 (4) (2012) 359–360.
[57] A. Al-Ansari, N. Younes, V.P. Sampige, K. Al-Rumaihi, A. Ghafouri, T. Gul, A. A. Shokeir, GreenLight HPS 120-W laser vaporization versus transurethral resection of the prostate for treatment of benign prostatic hyperplasia: a randomized clinical trial with midterm follow-up, Eur. Urol. 58 (3) (2010) 349–355, https://doi.org/10.1016/j.eururo.2010.05.026.
[58] B. Hu, Z. Song, H. Liu, L. Qiao, Y. Zhao, M. Wang, W. Song, D. Zhang, X. Jin, H. Zhang, A comparison of incidences of bladder neck contracture of 80- versus 180-W GreenLight laser photoselective vaporization of benign prostatic hyperplasia, Lasers Med. Sci. 31 (8) (2016) 1573–1581, https://doi.org/10.1007/s10103-016-2017-5.

[59] G.S. Steele, D.J. Sleep, Transurethral needle ablation of the prostate: a urodynamic based study with 2-year followup, J. Urol. 158 (5) (1997) 1834–1838, https://doi.org/10.1016/s0022-5347(01)64140-5.
[60] M.S. Soloway, E. Neulander, Bladder-neck preservation during radical retropubic prostatectomy, Semin. Urol. Oncol. 18 (1) (2000) 51–56.
[61] C.E. Brennen, Cavitation and Bubble Dynamics, Cambridge University Press, Cambridge, 2013.
[62] K.S. Suslick, S.J. Doktycz, E.B. Flint, On the origin of sonoluminescence and sonochemistry, Ultrasonics 28 (5) (1990) 280–290, https://doi.org/10.1016/0041-624x(90)90033-k.
[63] T.G. Leighton, 3 - The Freely-oscillating Bubble, in: T.G. Leighton (Ed.), The Acoustic Bubble, Academic Press, 1994, pp. 129–286.
[64] N.K. Gupta, S.N. Gange, K.T. McVary, New and Emerging Technologies in Treatment of Lower Urinary Tract Symptoms From Benign Prostatic Hyperplasia, Sex Med Rev 7 (3) (2019) 491–498, https://doi.org/10.1016/j.sxmr.2018.02.003.
[65] A. Ponholzer, M. Marszalek, S. Madersbacher, Minimally Invasive Treatment of BPH: An Update, EAU Updat. Ser. 2 (1) (2004) 24–33, https://doi.org/10.1016/j.euus.2004.01.002.
[66] S. Affas, F.M. Schäfer, K. Algarrahi, V. Cristofaro, M.P. Sullivan, X. Yang, K. Costa, B. Sack, M. Gharaee-Kermani, J.A. Macoska, G. Gundogdu, C. Seager, C. R. Estrada Jr., J.R. Mauney, Augmentation Cystoplasty of Diseased Porcine Bladders with Bi-Layer Silk Fibroin Grafts, Tissue Eng. A 25 (11–12) (2019) 855–866, https://doi.org/10.1089/ten.TEA.2018.0113.
[67] T.G. Tuttle, D.R. Morhardt, A.A. Poli, J.M. Park, E.M. Arruda, S. Roccabianca, Investigation of Fiber-Driven Mechanical Behavior of Human and Porcine Bladder Tissue Tested Under Identical Conditions, J. Biomech. Eng. 143 (11) (2021), https://doi.org/10.1115/1.4051525.
[68] E. Morales-Orcajo, T. Siebert, M. Böl, Location-dependent correlation between tissue structure and the mechanical behaviour of the urinary bladder, Acta Biomater. 75 (2018) 263–278, https://doi.org/10.1016/j.actbio.2018.05.014.
[69] M.S. Jokandan, F. Ajalloueian, M. Edinger, P.R. Stubbe, S. Baldursdottir, I. S. Chronakis, Bladder wall biomechanics: A comprehensive study on fresh porcine urinary bladder, J. Mech. Behav. Biomed. Mater. 79 (2018) 92–103, https://doi.org/10.1016/j.jmbbm.2017.11.034.
[70] P. Dahms, Dahiya, Lue, Tanagho, Composition and biomechanical properties of the bladder acellular matrix graft: comparative analysis in rat, pig and human, Br. J. Urol. 82 (3) (1998) 411–419, https://doi.org/10.1046/j.1464-410X.1998.00748.x.
[71] O.W. Hakenberg, C. Linne, A. Manseck, M.P. Wirth, Bladder wall thickness in normal adults and men with mild lower urinary tract symptoms and benign prostatic enlargement, Neurourol. Urodyn. 19 (5) (2000) 585–593, https://doi.org/10.1002/1520-6777(2000)19:5<585::aid-nau5>3.0.co;2-u.
[72] J.L. Caruso, Decomposition Changes in Bodies Recovered from Water, Acad Forensic Pathol 6(1) (2016) 19-27. 10.23907/2016.003.
[73] T.J. Ziemlewicz, J.L. Hinshaw, M.G. Lubner, E.A. Knott, B.J. Willey, F.T. Lee Jr., C. L. Brace, Radiofrequency and microwave ablation in a porcine liver model: non-contrast CT and ultrasound radiologic-pathologic correlation, Int. J. Hyperth. 37 (1) (2020) 799–807, https://doi.org/10.1080/02656736.2020.1784471.
[74] B. Becker, D. Enikeev, P. Glybochko, L. Rapoport, M. Taratkin, A.J. Gross, V. Vinnichenko, T.R.W. Herrmann, C. Netsch, Effect of optical fiber diameter and laser emission mode (cw vs pulse) on tissue damage profile using 1.94 μm Tm:fiber lasers in a porcine kidney model, World J Urol 38(6) (2020) 1563-1568. 10.1007/s00345-019-02944-y.
[75] M. Babaiasl, S. Boccelli, Y. Chen, F. Yang, J.L. Ding, J.P. Swensen, Predictive mechanics-based model for depth of cut (DOC) of waterjet in soft tissue for waterjet-assisted medical applications, Med. Biol. Eng. Compu. 58 (8) (2020) 1845–1872, https://doi.org/10.1007/s11517-020-02182-0.
[76] T. Bahls, F.A. Frohlich, A. Hellings, B. Deutschmann, A.O. Albu-Schaffer, Extending the Capability of Using a Waterjet in Surgical Interventions by the Use of Robotics, I.E.E.E. Trans. Biomed. Eng. 64 (2) (2017) 284–294, https://doi.org/10.1109/tbme.2016.2553720.
[77] H.G. Rau, A.P. Duessel, S. Wurzbacher, The use of water-jet dissection in open and laparoscopic liver resection, HPB (Oxford) 10 (4) (2008) 275–280, https://doi.org/10.1080/13651820802167706.
[78] O.Y. Perk, M. Şeşen, D. Gozuacik, A. Koşar, Kidney stone erosion by micro scale hydrodynamic cavitation and consequent kidney stone treatment, Ann. Biomed. Eng. 40 (9) (2012) 1895–1902, https://doi.org/10.1007/s10439-012-0559-7.
[79] D. Uzusen, E. Demir, O. Yavuz Perk, O. Oral, S. Ekici, M. Unel, D. Gozuacik, A. Kosar, Assessment of Probe-to-Specimen Distance Effect in Kidney Stone Treatment With Hydrodynamic Cavitation, J. Med. Devices 9 (3) (2015), https://doi.org/10.1115/1.4030274.
[80] Z. Itah, O. Oral, O.Y. Perk, M. Sesen, E. Demir, S. Erbil, A.I. Dogan-Ekici, S. Ekici, A. Kosar, D. Gozuacik, Hydrodynamic cavitation kills prostate cells and ablates benign prostatic hyperplasia tissue, Exp. Biol. Med. (Maywood) 238 (11) (2013) 1242–1250, https://doi.org/10.1177/1535370213503273.
[81] M.T. Gevari, G. Aydemir, G. Gharib, O. Kutlu, H. Uvet, M. Ghorbani, A. Koşar, Local Carpet Bombardment of Immobilized Cancer Cells With Hydrodynamic Cavitation, IEEE Access 9 (2021) 14983–14991, https://doi.org/10.1109/ACCESS.2021.3052893.
[82] I. Namli, Z. Karavelioglu, S.S. Sarraf, A.S. Aghdam, R. Varol, A. Yilmaz, S.B. Sahin, B. Ozogul, D.N. Bozkaya, H.F. Acar, H. Uvet, S. Çetinel, Ö. Kutlu, M. Ghorbani, A. Koşar, On the application of hydrodynamic cavitation on a chip in cellular injury and drug delivery, Lab Chip 23 (11) (2023) 2640–2653, https://doi.org/10.1039/D3LC00177F.
[83] H.C. Kim, A. Al-Mahrouki, A. Gorjizadeh, R. Karshafian, G.J. Czarnota, Effects of biophysical parameters in enhancing radiation responses of prostate tumors with ultrasound-stimulated microbubbles, Ultrasound Med. Biol. 39 (8) (2013) 1376–1387, https://doi.org/10.1016/j.ultrasmedbio.2013.01.012.
[84] M.A. Pimentel, O. Yassaie, P.J. Gilling, The Aquabeam System: a Review, Curr. Bladder Dysfunct. Rep. 13 (1) (2018) 1–7, https://doi.org/10.1007/s11884-018-0455-6.
[85] J.S. Engelsgjerd, C.M. Deibert, Cystoscopy, StatPearls, StatPearls Publishing Copyright © 2024, StatPearls Publishing LLC., Treasure Island (FL), 2024.
[86] A.L. de Castro Abreu, O. Ukimura, S. Shoji, S. Leslie, S. Chopra, A. Marien, T. Matsugasumi, A. Dharmaraja, K. Wong, N. Zaba, Y. Ma, M.M. Desai, I.S. Gill, Robotic transmural ablation of bladder tumors using high-intensity focused ultrasound: Experimental study, Int J Urol 23(6) (2016) 501-8. 10.1111/iju.13083.
[87] D.D. Nguyen, N. Barber, M. Bidair, P. Gilling, P. Anderson, K.C. Zorn, G. Badlani, M. Humphreys, S. Kaplan, R. Kaufman, A. So, R. Paterson, L. Goldenberg, D. Elterman, M. Desai, J. Lingeman, C. Roehrborn, N. Bhojani, Waterjet Ablation Therapy for Endoscopic Resection of prostate tissue trial (WATER) vs WATER II: comparing Aquablation therapy for benign prostatic hyperplasia in 30-80 and 80-150 mL prostates, BJU Int. 125 (1) (2020) 112–122, https://doi.org/10.1111/bju.14917.
[88] H.S. Ahn, S.J. Kim, J.B. Choi, S.H. Choo, K.H. Shim, S.I. Kim, Long-term cost comparison between surgical and medical therapy for benign prostatic hyperplasia: a study using hospital billing data, BJU Int. 123 (5a) (2019) E79–E85, https://doi.org/10.1111/bju.14584.